PHYSICAL REVIEW VOLUME 188, NUMBER 1 5 DECEMBER 10

X-Ray Scattering from Liquid Helium

Fugene K. Achter*† and Lothar Meyer
James Franck Institute and Department of Chemistry, The University of Chicago, Chicago, Illinois 60637
(Received 16 June 1969)

We have measured the liquid structure factor $S(k)$ for liquid He^4 and for liquid He^3 by x-ray diffraction. Our results for liquid He^4 agree with the Feynman formula $\hbar k/2mc$ in the range $0.3 < k < 0.6$ Å^{-1}, in contrast to previous measurements of $S(k)$ which fell about 25% below $\hbar k/2mc$ in this range. The peak in the pair distribution function $g(r)$ derived from the scattering data occurs at greater interatomic distance and is lower, broader, and less symmetrical for liquid He^3 than for liquid He^4, in agreement with predictions based on variational calculations. However, the experiments indicate slightly more structure in both liquids than the calculations predict. We have also measured $S(k)$ for He^4 vapor at 4.2 K, 0.98 atm. For He^4 vapor, $g(r)$ shows a distinct nearest-neighbor shell and probably a second-nearest-neighbor shell.

I. INTRODUCTION

We have been studying the structure of liquid helium by x-ray diffraction. In an x-ray diffraction experiment, monochromatic x-rays of wavelength λ impinge on the sample and the scattered x-ray intensity is measured as a function of scattering angle θ. The liquid-structure factor $S(k)$ is defined to give a measure of intermolecular correlations[1-3]

$$S(k) \equiv \frac{\text{Diffraction from } N \text{ atoms in sample}}{\text{Diffraction from } N \text{ isolated atoms}} . \quad (1)$$

k is the momentum change experienced by the scattered x-ray photon, and is given by $k = (4\pi/\lambda)(\sin\frac{1}{2}\theta)$. k has units of Å^{-1} and is determined by the scattering angle if the wavelength is known. $S(k)$ is related to the pair distribution function $g(r)$ by a Fourier transform[1-3]:

$$S(k) = 1 + (4\pi\rho/k)\int_0^\infty [g(r) - 1]\, r \sin kr\, dr . \quad (2)$$

For liquid helium, the behavior of $S(k)$ for small k is of considerable interest. $S(k)$ is the Fourier transform of density fluctuations present in the liquid and expressed in $g(r)$. Long-wavelength density fluctuations in a liquid are longitudinal sound waves. Hence a relationship exists between the structure factor $S(k)$ and the propagation of sound with wave vector k. If $E(k)$ is the excitation spectrum for phonons,

$$S(k) = \hbar^2 k^2/2mE(k) , \quad (3)$$

where m is the mass of one atom in the liquid.

This expression was derived by Bijl[4] and Feynman[5] using a variational wave function. It can also be derived using sum rules on the spectral function $S(k,\omega)$.[6] The derivation using sum rules assumes that $S(k,\omega)$ can be factored into a product of the form $S(k,\omega) = S(k)\delta(E - \hbar\omega)$.

If the excitations are simple phonons, one would expect that $E(k) = \hbar ck$, where c is the speed of sound. For liquid He^4, the excitation spectrum has been measured by inelastic neutron scattering.[7] The data show that for $k < 0.6$ Å^{-1}, $E = \hbar ck$ within experimental error of a few percent, implying that $S(k) = \hbar k/2mc$.

The foregoing is strictly true only at absolute zero. At finite temperatures, $S(k)$ must converge to $S(0) = \rho k_B T K_T$, where k_B is Boltzmann's constant and K_T is the isothermal compressibility. At temperatures around 1 K, this correction is unimportant for k greater than 0.3 Å^{-1}.[8] Thus, one would expect $S(k) = \hbar k/2mc$ to be valid for $0.3 < k < 0.6$ Å^{-1} at $T \sim 1$ K.

The structure factor for liquid He^4 has been measured by x-ray diffraction[9] and by neutron diffraction.[10] The results are reproduced in Fig. 1. The experimental $S(k)$ fall about 25% below $\hbar k/2mc$. The disagreement between theory and experiment is especially disturbing because the theory seems so straightforward.

By considering the neutron diffraction data only, it was predicted[11,12] that $S(k)$ would show a hump at $k \sim 0.7$ Å^{-1} and would converge to $\hbar k/2mc$ for $k \sim 0.5$ Å^{-1}.

In order to try to resolve the problem, we set out to remeasure $S(k)$ for liquid He^4 for small k.

By Fourier inversion of $S(k)$, one can obtain $g(r)$, the pair distribution function. The structure of a given liquid is determined by the balance of kinetic energy and intermolecular forces; hence $g(r)$ is related to the intermolecular forces. If one assumes that intermolecular forces can be adequately represented by a pair potential, static thermodynamic properties for a classical fluid can in principle be calculated from the pair dis-

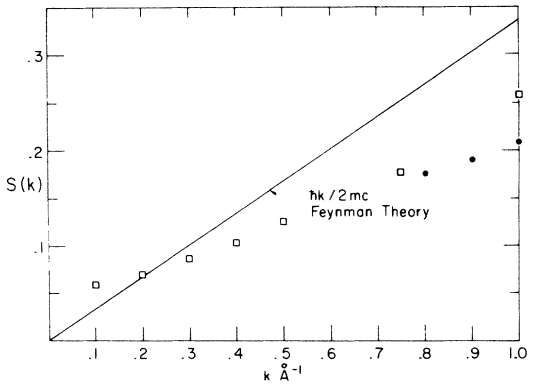

FIG. 1. Liquid-structure factor of liquid He^4 for small k. □, Gordon, Shaw, and Daunt (Ref. 8). ●, Henshaw (Ref. 9).

tribution function and the intermolecular potential. Alternatively, the pair distribution function and thermodynamic properties can be determined variationally for a given choice of pair potential.[13]

Similar variational calculations are possible for quantum fluids. From a given pair potential and a variational wave function the pair distribution function and properties such as the binding energy can be obtained. However, knowledge of the pair distribution function and the pair potential is not sufficient to determine the binding energy; for a quantum fluid, the wave function is needed to calculate the zero-point energy.[13]

He^4 is a boson fluid boiling at 4.2 K, becoming superfluid below 2.2 K, with binding energy − 7.14 K/atom. He^3 is a fermion fluid boiling at 3.2 K, with binding energy -2.53 K/atom.[14] The interatomic potential depends on electronic structure and should be the same for He^3 and He^4. Thus, a comparison of He^3 and He^4 properties sheds direct light on the effects of quantum statistics.

Several variational calculations of the pair distribution function and binding energy for He^4 and He^3 have recently been reported.[15–18] Calculations for He^4 and for a hypothetical mass-3 boson fluid were made using Jastrow trial wave functions[19] and Lennard-Jones (LJ) 6-12 pair potentials. Solutions for fermion He^3 were obtained from the boson He^3 results using cluster-expansion techniques developed by Wu and Feenberg.[20]

Massey[16] obtained solutions for He^4 and for boson He^3 by means of the Bogoliubov-Born-Green-Kirkwood-Yvon equation.[19] He adjusted the LJ pair potential for He^4 to obtain agreement with experimental values for the density and binding energy at absolute zero. This adjusted LJ pair potential was then used for the boson He^3 calculation. Woo[17] used Massey's boson He^3 results in his calculation for fermion He^3.

McMillan[15] reported Monte Carlo calculations for He^4 using a LJ potential determined from virial coefficients by DeBoer and Michels.[21] Schiff and Verlet[18] used the same LJ potential in molecular dynamics calculations for He^4 and for boson He^3. From these boson He^3 results, they calculated various properties for fermion He^3.

Massey and Woo[22] have repeated their calculations using the DeBoer-Michels potential chosen by Schiff and Verlet, obtaining results very close to those of Schiff and Verlet. The results are more sensitive to choice of potential than to the method of calculation. Sim and Woo[23] have recently evaluated corrections to the Kirkwood superposition approximation numerically.

The pair distribution functions obtained in the calculations cited above are in good agreement. The results indicate that the peak in $g(r)$ will be lower and broader, and will occur at greater r for He^3 than for He^4. This is due in part to the lighter mass and greater zero-point energy of He^3 and in part to the effective repulsions of Fermi statistics.

We set out to measure $S(k)$ for both He^3 and He^4 at low temperatures using the same apparatus in order to compare the pair distribution functions empirically.

II. EXPERIMENTAL

In the experiment, a monochromatic x-ray beam impinges on a sample of liquid or gaseous helium, and the scattered intensity is measured as a function of scattering angle. The sample is maintained at cryogenic temperatures by using a He^3 refrigerator (see Fig. 2). The cryostat and x-

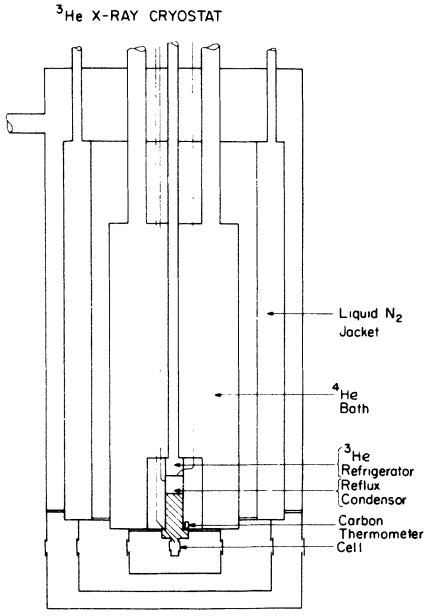

FIG. 2. He^3 x-ray cryostat.

ray monochromator were first constructed by Narahara, who has published preliminary results of x-ray scattering from liquid He^3.[24] We have been able to make considerable improvements based on his experiences.

The sample cell consisted of a copper chamber with windows transparent to x rays. For measurements over a wide angular range, we used a cell with cylindrical walls of 0.002-in. Mylar. For small-angle measurements, a cell with flat Be windows was used. Sample temperature was measured by a carbon-resistor thermometer attached to the copper wall of the cell. The thermometer was calibrated against the vapor pressure of He^4 or He^3 in the cell, using an Octoil-s oil manometer.

The cell is surrounded by heavy copper radiation shields anchored to the He^4 chamber and the nitrogen jacket, respectively. X-ray transparency is provided by 0.002-in. Be windows sealed to the radiation shields and the outer vacuum jacket with Epoxy. A more detailed description of the apparatus is available.[25]

The cryostat is mounted on a goniometer in such a way that the center of the cell coincides with the axis of the goniometer. A copper target x-ray tube is energized using a constant potential, current-stabilized power supply (typical settings were 50 kV-11 mA). Scattered x rays are detected using a Li I scintillation detector, a single-channel pulse-height analyzer, and pulse counting circuitry. The odometer of the goniometer reads one hundredths of a degree. The goniometer arm is motor driven, and the system can be set to stop automatically at 1° intervals, count for a preset time of number of pulses, print out time and counts, and go on to the next angle.

In order to determine $k = (4\pi/\lambda)\sin\frac{1}{2}\theta$, the scattering angle and the wavelength must both be well defined. For measurements over a large angular range, we obtained a monochromatic, focused Cu $K\alpha$ x-ray beam using a bent Li F monochromator constructed by Cohen and Morrison of Northwestern University.[26] For the small-angle measurements, we used a beam that was well collimated by an arrangement of slits. To ensure monochromatic x rays, we used a Ni filter 0.0018 in. thick to filter out the $K\beta$ line and a pulse-height analyzer to discriminate against the short-wavelength white radiation.

III. DATA ANALYSIS

X rays are scattered by the electrons in matter, so the scattering depends on the electronic structure. Some of the scattering is incoherent, which means that the x-ray photon is scattered with random phase. Diffraction requires phase coherence; therefore incoherent scattering does not contribute to diffraction, and corrections must be made. Structural information is contained in coherent, or in-phase, scattering. The coherent scattering stems from the electron density distribution for the whole sample, and can be factored into intra-atomic and interatomic contributions. When corrections have been made for incoherent scattering and for intraatomic coherent scattering, one can obtain information about interatomic distributions.

For a system of isolated atoms,[1-3] the number of x-ray photons scattered with momentum change $k = (4\pi/\lambda)\sin\frac{1}{2}\theta$ is proportional to

$$V(\theta)\rho[\,|F_{\rm coh}(k)|^2 + F_{\rm inc}(k)]\sigma_{\rm th}A(\theta)\,. \qquad (4)$$

In this expression, $\sigma_{\rm th}$ is the Thomson scattering cross section for a free electron, and is given by

$$\sigma_{\rm th} = (e^4/2m^2c^4)(1+\cos^2\theta)\,.$$

If a monochromator crystal is used, the beam is polarized before it impinges on the sample, and

$$\sigma_{\rm th} = (e^4/2mc^4)(1+\cos^2\theta\cos\phi_m)/(1+2\cos\phi_m)\,, \qquad (5)$$

where ϕ_m is the Bragg angle for the monochromator.

$V(\theta)$ is the number of atoms in the sample volume illuminated by the main beam and accessible to the detector slits. While the angular dependence of $V(\theta)$ can be calculated for idealized slit configurations,[27] these calculations assume conditions of slit resolution, beam uniformity, and physical alignment that may not be realized in practice. For greater accuracy, we have determined $V(\theta)$ by empirical means, which will be discussed below.

$A(\theta)$ compensates for intensity loss due to absorption or multiple scattering of x rays by the sample. In passing through $\frac{1}{4}$ in. of liquid helium, a Cu $K\alpha$ x-ray beam suffers intensity loss of only 3%, so $A(\theta)$ can safely be evaluated using standard formulas for a uniform thin x-ray beam.[28]

$F_{\rm coh}(k)$ is the atomic form factor and $F_{\rm inc}(k)$ is the incoherent scattering function. They can be obtained from a variational ground-state wave function for a given atom.

For a system of atoms with spatial correlations,[1-3] the scattering is proportional to

$$V(\theta)\rho[\,|F_{\rm coh}(k)|^2 S(k) + F_{\rm inc}(k)]\sigma_{\rm th}A(\theta)\,. \qquad (6)$$

As long as free atom wave functions can be used to describe the atoms in the sample, the free-atom values for $F_{\rm coh}$ and $F_{\rm inc}$ can be used. This assumption is reasonable since the interatomic interaction energy is negligible compared to the electronic binding energy of the atom. If

the free-atom F_{coh} and F_{inc} can be used and the sample is isotropic, the equation

$$S(k) = 1 + (4\pi\rho/k)\int_0^\infty [g(r) - 1] r \sin kr\, dr \qquad (7)$$

can be derived without any assumptions about three-body and higher interactions.

$I_{exp}(\theta)$ is the experimental intensity in counts/sec observed at angle θ, less scattering from the empty cell at that angle.

$$I_{exp}(\theta) = V(\theta)\rho[|F_{coh}(k)|^2 S(k) + F_{inc}(k)]A(\theta). \qquad (8)$$

$V(\theta)$ can be determined empirically by measuring scattering from an ideal gas, for which $S(k) = 1.00$. For the ideal gas, we used neon at 77 K, 1 atm, for which we calculate $S(0) = 1.005$ from virial coefficients.[29] The scattered intensity from neon gas at 77 K, 1 atm was of the same order of magnitude as that from helium gas and helium liquid. This is because the atomic scattering cross section varies roughly as the square of the atomic number, so the greater scattering per atom for neon compensated for the lower density of neon gas at 77 K, 1 atm. Incidentally, for small angles, the total scattering from either neon gas or helium gas exceeded that from liquid helium; scattering from the liquid is proportional to $S(k)$, which becomes very small for small k. The absorption correction for the neon sample was about 4%, compared with 3% for the liquid-helium sample.

For helium, we used F_{coh} and F_{inc} calculated by Kim and Inokuti from the 20-term Hylleraas wave function.[30] For neon, values of F_{coh} and F_{inc} calculated by Tavard, Nicolas, and Roualt[31] from the Clementi Hartree-Fock self-consistent-field (HF-SCF) wave function were used. Densities were obtained from published PVT data for neon,[29] liquid He^3,[32] liquid He^4,[33] and He^4 gas.[34] We determined absorption corrections using published attenuation coefficients for He and for Ne.[35]

In a typical experiment, we would measure x-ray scattering from the sample and from the empty cell at 1° intervals, counting for at least 10^4 counts at each scattering angle. As a check against drift in the x-ray generating and detecting apparatus, we recounted at various angular positions during the course of each run, and compared cell background levels from day to day.

To determine $S(k)$ for liquid He^4 for small k, we used a filtered collimated x-ray beam and the flat cell with Be windows. The full width at half-height of the beam profile was 0.3°. The counter slits were 50 mil wide, and the over-all angular resolution was about 0.5°. We measured x-ray scattering from liquid He^4 at 1 K and from neon gas at 77 K, 1 atm, and determined $S(k)$ for liquid He^4 directly. The neon-gas measurements

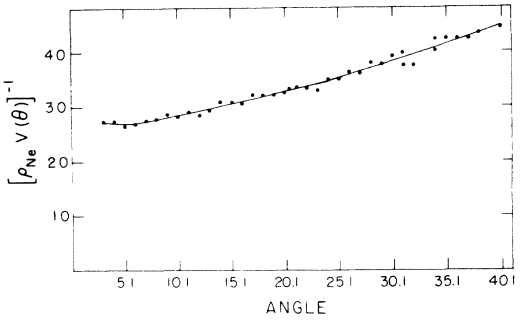

FIG. 3. Calibration of scattering volume correction obtained from the neon-gas experiment. $[\rho_{Ne} V(\theta)]^{-1}$ in relative units is plotted as a function of scattering angle.

extended to $k = 2.5$ Å^{-1}. Scattering from He^4 gas at 4.2 K, 0.98 atm, was also measured for k up to 2.25 Å^{-1}, and $S(k)$ for He^4 gas was determined using the neon data for calibration.

The calibration curve $\rho_{Ne} V(\theta)$ obtained from the neon scattering experiment is shown in Fig. 3. Our measurements of $S(k)$ for He^4 gas at 4.2 K, 0.98 atm, are shown in Fig. 4. The quantity

$$\lim_{k \to 0} S(k) = \rho k T K_T$$

was calculated from the Leiden virial coefficients.[34] A smooth curve is drawn through the experimental points. Despite the scatter in the data, it is quite clear that $S(k)$ is considerably greater than unity for small k. Furthermore, $S(k)$ seems to dip below unity at $k \sim 1.1$ Å^{-1} and to peak slightly at $k \sim 1.8$ Å^{-1}. Gordon, Shaw and Daunt[9] calibrated their apparatus using He^4 gas at 4.2 K, 0.46 atm, for which we calculate $S(0) = 1.3$ from the Leiden virial coefficients. If the apparatus is calibrated using a gas for which $S(k)$ is greater than unity, the values of $S(k)$ obtained for the liquid sample

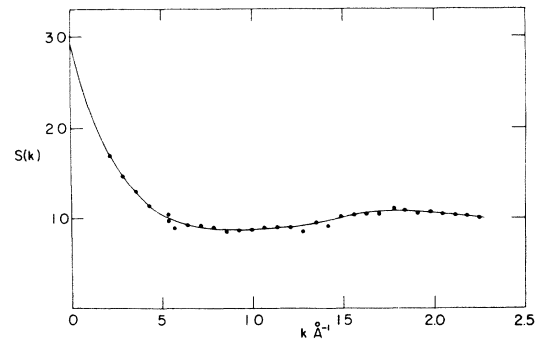

FIG. 4. $S(k)$ for He^4 gas at 4.2 K, 0.98 atm.

will be too small.

$S(k)$ for He^4 gas at $p \sim 0.5$ atm, $T = 4.0$ K has been calculated by Lee using integral equation methods developed for quantum fluids.[36] These results are consistent with our data. We wish to thank Dr. Lee for making his unpublished results available to us.

We used $S(k)$ for He^4 gas at 4.2 K, 0.98 atm to compute the pair distribution function $g(r)$, shown in Fig. 5. Because of the scatter in the data, the smooth curve for $S(k)$ is uncertain by about $\pm 2\%$ of $S(k)$. For $0.5 < k < 2.5$ Å^{-1}, this amounts to $\pm 20\%$ error in $S(k) - 1$. $g(r)$ is obtained as the Fourier transform of $S(k) - 1$, so the uncertainty in $g(r)$ is considerable. However, the qualitative similarity between our $g(r)$ for He^4 gas and the results of Mikolaj and Pings[37] for argon gas at $t = -125$ °C, $\rho = 0.280$ g/cc is striking.

To measure $S(k)$ for liquid He^4 and for liquid He^3 in the range $0.3 < k < 4$ Å^{-1}, we used a LiF monochromator and the cylindrical cell with Mylar walls. Because of the divergence of the main beam, the angular resolution was about 1°. To normalize the liquid data, we measured scattering from He^4 gas at 4.2 K using the same experimental configuration. Later, when we realized that $S(k)$ for He^4 gas deviates very seriously from unity, we used the experimental $S(k)$ for He^4 gas determined via the neon-gas experiments to correct the liquid He^4 and He^3 results.

RESULTS

We have measured $S(k)$ for liquid He^4 for small k in the flat cell in order to check the apparent deviations from Feynman's theory. Earlier measurements by x ray[9] and by neutron diffraction[10] indicated that $S(k)$ falls about 25% below $\hbar k/2mc$. Our data appear in Fig. 6. For $0.3 < k < 0.6$ Å^{-1}, they confirm Feynman's theory within experimental error of a few percent. The most likely reason that our $S(k)$ differ from the previous measurements is that we determined the scattering volume correction $V(\theta)$ empirically, using a really ideal gas.

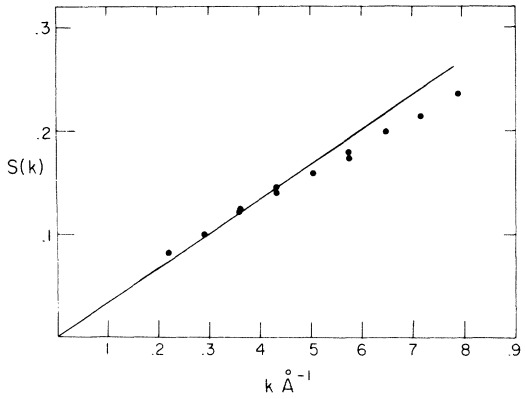

FIG. 6. $S(k)$ for liquid He^4 for small k. $T = 1.1$ K.

For $0.5 < k < 1.0$ Å^{-1}, our data fall slightly below $\hbar k/2mc$. From perturbation calculations Lee[38] obtained the result $E(k) = (1 - 0.334k^2)\hbar k/2mS(k)$, implying that $S(k) \leq \hbar k/2mc(1 - 0.17k^2)$.[39] Our measurements are consistent with this expression, but a systematic error sufficient to produce the observed deviation from $\hbar k/2mc$ cannot be ruled out. We measured $S(k)$ throughout the range $0.3k < 1.0$ Å^{-1}, but we found no evidence for the hump in $S(k)$ predicted in this range by Miller, Pines, and Nozieres,[11] and by Massey.[12]

Our other main objective was to obtain and compare the pair distribution functions for liquid He^3 and liquid He^4. We measured x-ray scattering for angles up to 80° to obtain $S(k)$ for k greater than 4.0 Å^{-1}, using the Mylar cell and the LiF monochromator. Our results for $S(k)$ are shown in Figs. 7 and 8. The peak in $S(k)$ occurs at $k = 2.05$ Å^{-1} for He^4 and at $k = 1.90$ Å^{-1} for He^3. The blank spaces were experimentally inaccessible

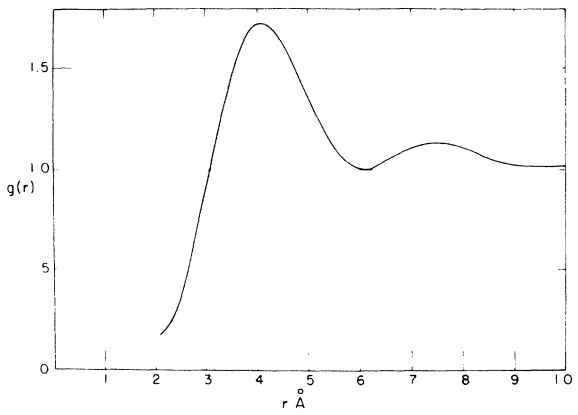

FIG. 5. $g(r)$ for He^4 gas at 4.2 K, 0.98 atm.

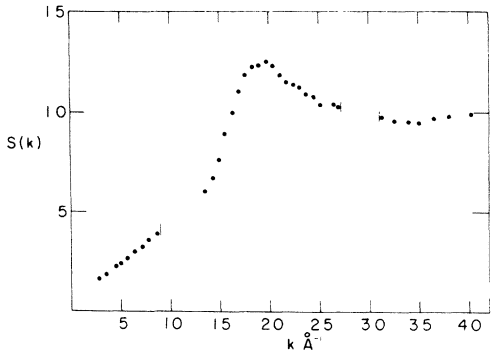

FIG. 7. $S(k)$ for liquid He^3. $T = 0.56$ K.

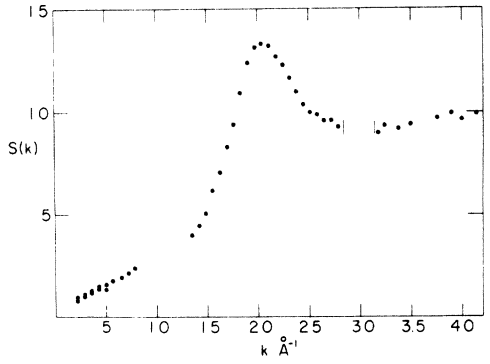

FIG. 8. $S(k)$ for liquid He^4. $T=0.79$ K.

because of Mylar peaks in the cell background. Narahara's preliminary data for liquid He^3 [34] are consistent with the present results, but his data are considerably less precise.

For k greater than 3, there is considerable scatter in the data. This is because, for large k, the total x-ray scattering becomes very small and largely incoherent, so that the coherent scattering is only a small fraction of a small value.

$g(r)$ is obtained from $S(k)$ by the equation

$$g(r)=1+(2\pi^2/r\rho)\int_0^\infty [S(k)-1]k\sin kr\,dk \quad . \quad (9)$$

In order to get a meaningful Fourier transform we drew a smooth curve through the graph for $S(k)$, in effect averaging the statistical scatter. Since $\sin kr$ can sometimes do strange things when it is approximated by a polynomial, we partitioned the curve into increments small enough so that $S(k)$ was locally linear, and we evaluated

$$\int_{k_1}^{k_2} [S(k)-1]k\sin kr\,dk$$

analytically for each interval. The smoothed values of $S(k)$ obtained for He^4 and for He^3 are listed in Tables I and II. In Table III, the peak height and peak position of $S(k)$ for He^4 are compared with earlier measurements by other authors.

The Fourier integral has an infinite upper limit, and the true $S(k)$ undergoes diminishing oscillations in the limit $k\to\infty$. In practice, the integral must be terminated at some finite value of k. The effect of this so-called termination error is to introduce spurious ripples in $g(r)$ for small r.[2] For r less than an at. diam, $g(r)=0$, so we can identify and reject the ripples as having no physical meaning. For $r>2$ Å, no such ripples were observed.

The pair distribution functions we obtained for He^3 and for He^4 are presented in Fig. 9 and in Tables IV and V. For purposes of comparison, the results of Massey[16] and Woo[17] are reproduced in Figs. 10 and 11.

Our data show that the first maximum in $g(r)$ is lower, broader, and occurs at greater r for He^3 than for He^4, in excellent qualitative agreement with the theoretical calculations.

TABLE I. $S(k)$ for liquid He^4, $T=0.79$ K.

k (Å^{-1})	$S(k)$
0	0.027
0.20	0.075
0.40	0.135
0.60	0.185
0.80	0.230
1.00	0.285
1.20	0.345
1.30	0.380
1.40	0.435
1.50	0.525
1.60	0.675
1.70	0.850
1.80	1.025
1.90	1.240
1.92	1.280
1.94	1.300
1.96	1.310
1.98	1.320
2.00	1.325
2.04	1.330
2.10	1.323
2.12	1.320
2.20	1.260
2.30	1.175
2.40	1.085
2.45	1.040
2.50	1.016
2.60	0.983
2.70	0.970
2.80	0.945
2.90	0.933
3.00	0.927
3.10	0.921
3.20	0.920
3.30	0.921
3.40	0.923
3.50	0.929
3.60	0.933
3.70	0.940
3.80	0.950
3.90	0.958
4.00	0.968
4.10	0.980
4.20	0.997
4.30	1.000
4.50	1.000

TABLE II. $S(k)$ for liquid He^3, $T=0.56$ K.

k(Å^{-1})	$S(k)$
0	0.047
0.10	0.090
0.20	0.127
0.40	0.200
0.60	0.285
0.80	0.363
1.00	0.440
1.10	0.475
1.20	0.525
1.30	0.575
1.35	0.600
1.40	0.640
1.44	0.670
1.50	0.790
1.60	0.965
1.70	1.105
1.76	1.185
1.83	1.225
1.90	1.241
1.95	1.247
2.00	1.237
2.05	1.225
2.10	1.200
2.20	1.155
2.30	1.120
2.40	1.087
2.50	1.055
2.60	1.035
2.70	1.017
2.80	1.000
2.90	0.988
3.00	0.979
3.10	0.970
3.20	0.962
3.30	0.957
3.40	0.955
3.50	0.960
3.60	0.968
3.80	0.981
4.00	0.994
4.08	1.000
4.20	1.000

TABLE III. Structure factor for He^4.

k_m(Å^{-1})	$S(k_m)$	Source
2.04 ± 0.03	1.33 ± 0.03	This work
2.00	1.42	Gordon, Shaw, and Daunt[a]
2.05	1.50	Henshaw[b]

[a]Reference 9.
[b]Reference 10.

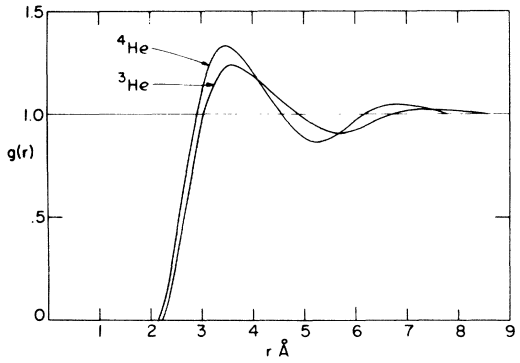

FIG. 9. $g(r)$ for He^3 at $T=0.56$ K and He^4 at $T=0.79$ K.

The experimental $g(r)$ show a more pronounced structure than predicted theoretically – the first maxima are higher, and second-nearest-neighbor peaks are clearly evident. In Tables VI and VII, the experimental and theoretical peak heights and nearest-neighbor distances are compared. Our data for He^4 agree very closely with the calculation: For He^3, the first peak in our $g(r)$ shows substantially greater height and smaller nearest-neighbor distance than predicted.

The degree of structure exhibited in $g(r)$ as indicated by peak height and position should be closely related to the binding energy – the greater the binding energy, the more pronounced the structure. In the calculations, the binding energy is obtained as a small difference between kinetic and potential energy. The calculated binding energies and densities are compared with experimental values in Tables VIII and IX. For He^4, the binding energy is underestimated by up to 15% and the density by 10%. For He^3, the binding energy is underestimated by 45% and the density by 13%. Thus, it is not surprising that the calculations underestimate the degree of structure in $g(r)$ more seriously for He^3 than for He^4.

ACKNOWLEDGMENTS

We wish to thank Professor C. S. Barrett for valuable advice; Professor S. A. Rice and Professor K. Freed for helpful discussions; Professor E. Feenberg for valuable comments; and R. Szara for technical assistance. This research was supported in part by the National Science Foundation Grant No. GP8375 Res. and by facilities at the University of Chicago provided by the Advanced Research Projects Agency. Some of the equipment was contributed by Professor Barrett and by Professor Rice.

TABLE IV. $g(r)$ for liquid He^3, $T = 0.56$ K.

r(Å)	$g(r)-1$	r(Å)	$g(r)-1$
2.00	−1.129	6.00	−0.073
2.10	−1.098	6.10	−0.063
2.20	−1.037	6.20	−0.052
2.30	−0.948	6.30	−0.041
2.40	−0.835	6.40	−0.029
2.50	−0.707	6.50	−0.018
2.60	−0.569	6.60	−0.008
2.70	−0.428	6.70	0.000
2.80	−0.291	6.80	0.008
2.90	−0.163	6.90	0.014
3.00	−0.051	7.00	0.018
3.10	0.044	7.10	0.022
3.20	0.119	7.20	0.024
3.30	0.175	7.30	0.026
3.40	0.212	7.40	0.027
3.50	0.232	7.50	0.027
3.60	0.238	7.60	0.026
3.70	0.233	7.70	0.025
3.80	0.221	7.80	0.024
3.90	0.203	7.90	0.022
4.00	0.182	8.00	0.020
4.10	0.166	8.10	−0.016
4.20	0.139	8.20	−0.020
4.30	0.117	8.30	−0.023
4.40	0.097	8.40	−0.024
4.50	0.077	8.50	−0.024
4.60	0.058	8.60	−0.023
4.70	0.039	8.70	−0.020
4.80	0.020	8.80	−0.017
4.90	0.002	8.90	−0.013
5.00	−0.016	9.00	−0.010
5.10	−0.034	9.10	−0.006
5.20	−0.050	9.20	−0.003
5.30	−0.064	9.30	0.000
5.40	−0.075	9.40	0.002
5.50	−0.083	9.50	0.004
5.60	−0.088	9.60	0.005
5.70	−0.089	9.70	0.006
5.80	−0.086	9.80	0.006
5.90	−0.081	9.90	0.006

TABLE V. $g(r)$ for liquid He^4, $T = 0.79$ K.

r(Å)	$g(r)-1$	r(Å)	$g(r)-1$
2.00	−1.061	6.00	−0.029
2.10	−1.033	6.10	−0.010
2.20	−0.968	6.20	0.007
2.30	−0.869	6.30	0.020
2.40	−0.744	6.40	0.031
2.50	−0.599	6.50	0.039
2.60	−0.444	6.60	0.045
2.70	−0.288	6.70	0.048
2.80	−0.141	6.80	0.049
2.90	−0.008	6.90	0.048
3.00	0.106	7.00	0.046
3.10	0.195	7.10	0.043
3.20	0.261	7.20	0.039
3.30	0.304	7.30	0.034
3.40	0.326	7.40	0.029
3.50	0.329	7.50	0.023
3.60	0.319	7.60	0.016
3.70	0.298	7.70	0.025
3.80	0.270	7.80	0.024
3.90	0.237	7.90	0.022
4.00	0.202	8.00	0.020
4.10	0.166	8.10	0.017
4.20	0.129	8.20	0.014
4.30	0.094	8.30	0.001
4.40	0.059	8.40	0.008
4.50	0.025	8.50	0.005
4.60	−0.008	8.60	0.002
4.70	−0.038	8.70	−0.001
4.80	−0.066	8.80	−0.003
4.90	−0.090	8.90	−0.006
5.00	−0.109	9.00	−0.007
5.10	−0.123	9.10	−0.009
5.20	−0.132	9.20	−0.010
5.30	−0.134	9.30	−0.011
5.40	−0.130	9.40	−0.011
5.50	−0.120	9.50	−0.011
5.60	−0.106	9.60	−0.011
5.70	−0.089	9.70	−0.011
5.80	−0.069	9.80	−0.010
5.90	−0.049	9.90	−0.009

TABLE VI. Pair distribution function for He^4.

r_m	$g(r_m)$	Source
3.48	1.31	Massey
~3.5	1.27	McMillan
3.4	1.27	Schiff and Verlet
3.47 ± 0.05	1.33 ± 0.03	Experimental – this work
3.4	1.42	Experimental – Henshaw[a]

[a]Reference 10.

TABLE VII. Pair distribution function for He^3.

r_m	$g(r_m)$	Source
3.9	1.13	Woo
3.8	1.13	Schiff and Verlet[a]
3.6 ± 0.05	1.24 ± 0.03	Experimental – this work

[a]Reference 18.

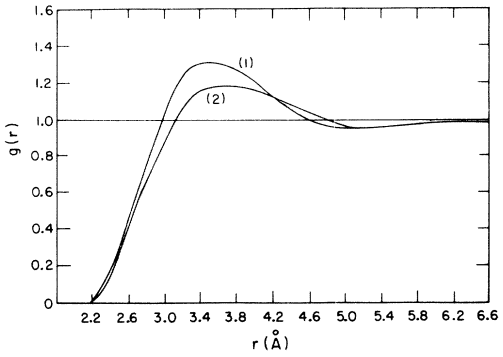

FIG. 10. $g(r)$ calculated by Massey (Ref. 16). (1) He^4. (2) boson He^3.

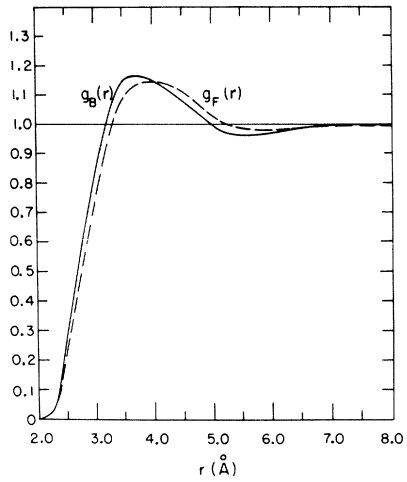

FIG. 11. $g(r)$ calculated by Woo (Ref. 17). $g_B(r)$, boson He^3. $g_F(r)$, fermion He^3.

TABLE VIII. Comparison of He^4 calculations.

Source	ρ/ρ_0	E_0(°K/atom)
Experimental	1	−7.14
McMillan[a]	0.89	−5.9
Schiff and Verlet[b]	0.9	−5.95
Massey[c]	fitted	fitted

[a]Reference 15.
[b]Reference 18.
[c]Reference 16.

TABLE IX. Comparison of fermion He^3 calculations.

Source	ρ/ρ_0	E_0(°K/atom)
Woo[a]	0.675	−1.35
Schiff and Verlet[b]	0.65	−1.35
Experimental	1	−2.52

[a]Reference 17.
[b]Reference 18.

*Submitted in partial fulfillment of the requirements for the Ph.D. degree at the University of Chicago.

†Present address: National Institute of Arthritis and Metabolic Diseases, National Institutes of Health, Bethesda, Md. 20014.

[1]N. Gingrich, Rev. Mod. Phys. 15, 90 (1943).
[2]K. Furukawa, Reports on Progress in Physics XXV (Institute of Physics and Physical Society, London, 1962), p. 395.
[3]H. H. Paalman and C. J. Pings, Rev. Mod. Phys. 35, 389 (1963).
[4]A. Bijl, Physica 7, 869 (1940).
[5]R. P. Feynman, Phys. Rev. 94, 262 (1954).
[6]P. Nozieres and D. Pines, Phys. Rev. 109, 741 (1958).
[7]D. G. Henshaw and A. D. B. Woods, Phys. Rev. 121, 1266 (1961).
[8]R. P. Feynman and M. Cohen, Phys. Rev. 102, 1189 (1956).
[9]W. L. Gordon, C. H. Shaw, and J. G. Daunt, J. Phys. Chem. Solids 5, 117 (1958).
[10]D. G. Henshaw, Phys. Rev. 119, 9 (1960).
[11]A. Miller, D. Pines, and P. Nozieres, Phys. Rev. 127, 1452 (1962).
[12]W. E. Massey, Phys. Rev. Letters 12, 719 (1964).
[13]Peter A. Egelstaff, An Introduction to the Liquid State (Academic Press Inc., London, 1967).
[14]K. R. Atkins, Liquid Helium (Cambridge University Press, Cambridge, England, 1959).
[15]W. L. McMillan, Phys. Rev. 138, 442 (1965).
[16]W. E. Massey, Phys. Rev. 151, 153 (1966).
[17]C. W. Woo, Phys. Rev. 151, 138 (1966).
[18]D. Schiff and L. Verlet, Phys. Rev. 160, 208 (1967).
[19]R. Jastrow, in The Many-Body Problem, edited by J. Percus (Wiley-Interscience, Inc., New York, 1963).
[20]F. Y. Wu and E. Feenberg, Phys. Rev. 128, 943 (1962).
[21]J. DeBoer and A. Michels, Physica 5, 945 (1938).
[22]W. E. Massey and C. W. Woo, Phys. Rev. 164, 256 (1967).
[23]H. K. Sim and C. W. Woo, Phys. Rev. 185, 401 (1969).
[24]Y. Narahara, J. Phys. Soc. Japan 24, 169 (1968).
[25]E. K. Achter, Ph.D. dissertation, University of Chicago, 1969 (unpublished).
[26]L. H. Schwartz, L. A. Morrison, and J. B. Cohen, in Advances in X-Ray Analysis, edited by William M. Meullers, Gavin Mallett, and Marie Fay (Plenum Press, New York, 1964), Vol. 7, p. 281.

[27]H. W. Furmoto, Ph.D. dissertation, Ohio State University, University Microfilms, Inc., Ann Arbor, Mich., 1963, p. 54 (unpublished).
[28]International Tables for X-Ray Crystallography (Kynoch Press, Birmingham, England, 1959), Vol. II, Chap. 5.3.
[29]J. A. Beattie, in Argon, Helium, and the Rare Gases, edited by G. Cook (Wiley-Interscience, New York, 1961), p. 262.
[30]Y. R. Kim and M. Inokuti, Phys. Rev. 165, 39 (1967).
[31]C. Tavard, D. Nicoles, and M. Rouault, J. Chem. Phys. 64, 541 (1967).
[32]E. C. Kerr and R. D. Taylor, Ann. Phys. (N.Y.) 20, 450 (1962).
[33]E. C. Kerr and R. D. Taylor, Ann. Phys. (N.Y.) 26, 292 (1964).
[34]W. H. Keesom and W. K. Walstra, Physica 7, 985 (1940).
[35]See Ref. 28, Vol. III, Chap. 3.2.
[36]M. Howard Lee (unpublished).
[37]P. G. Mikolaj and C. J. Pings, J. Chem. Phys. 46, 1401 (1967).
[38]D. K. Lee, Phys. Rev. 162, 134 (1967).
[39]E. Feenberg (private communication).

PHYSICAL REVIEW VOLUME 188, NUMBER 1 5 DECEMBER 1969

Observation of Neutrons Produced by Laser Irradiation of Lithium Deuteride†

G. W. Gobeli, J. C. Bushnell, P. S. Peercy, and E. D. Jones
Sandia Laboratories, Albuquerque, New Mexico 87115
(Received 11 July 1969)

The observation of neutrons produced by irradiation of polycrystalline LiD targets with a high-power laser is reported. Single pulses from a mode-locked Nd^{+3}-doped glass laser were amplified up to energies of 25 J. Pulse widths were 2–3 psec as measured by the two-photon fluorescence technique. The analyses of these experiments yield a somewhat higher rate of neutron production than the similar experiments recently reported by Basov *et al.*

There has been considerable interest concerning the possibility of laser-induced thermonuclear reactions since high-temperature plasmas have been produced by focused laser irradiation of solids in vacuum.[1] Recently, Basov *et al.*[2] have reported the observation of neutron production in a lithium deuteride sample when subjected to focused radiation from a high-power laser pulse. We report in this paper the results and interpretations of a similar investigation using a large 1.06-μ Nd^{+3}-doped glass laser. In our experiments, the laser pulse was focused onto the surface of polycrystalline LiD in vacuum and incident energies up to 25 J in a single pulse of duration of the order of 3 psec were used. A large pilot B scintillation counter encased in $\frac{1}{16}$-in. aluminum was time gated in order to look for counting events immediately following the laser pulse arrival at the target.

The single optical pulse was selectively gated from the train of pulses produced by a mode-locked oscillator and subsequently amplified to multijoule energy. The oscillator consisted of a 1-cm-diam × 15-cm-long double Brewster Nd^{+3}-doped glass rod pumped in close-coupled configuration. Maximum reflectivity (> 99.8%) and 55% reflectivity plano mirrors formed the optical cavity, and Eastman Kodak 9860 bleachable dye was used as the passive mode-locking Q-switching element. The optical cavity was 2.2 m long, giving an interpulse spacing in the output train of ~15 nsec. Very clean optical pulse trains having a total duration of 400 nsec were obtained when the laser was properly aligned. Care was taken to slightly tilt all reflective surfaces both inside and outside the cavity to prevent feedback to the oscillator, since such feedback was found to degrade the quality of mode locking. The time duration of the optical pulses are estimated by the use of two-photon fluorescence (TPF) in rhodamine 6 G.[3] "Properly" mode-locked pulses exhibited a single bright line with full width at half-maximum above the background of 1.0–1.3 psec and contrast ratio of approximately 2. No shoulders or low intensity blurring of the patterns were found in such cases. Subject to clarification of the interpretation of TPF data,[4–6] the pulse width delivered by this laser when properly mode locked, will be designated in terms of the TPF patterns and is nominally 2–3 psec.